Progress in the Understanding of Drug–Receptor Interactions, Part 1: Experimental Charge-Density Study of an Angiotensin II Receptor Antagonist ($C_{30}H_{30}N_6O_3S$) at $T = 17$ K

Riccardo Destro,*[a] Raffaella Soave,[b] Mario Barzaghi,[b] and Leonardo Lo Presti[a]

Dedicated to Dr. Richard E. Marsh on the occasion of his 83rd birthday

Abstract: An experimental study of the electron-density distribution $\rho(\boldsymbol{r})$ in an angiotensin II receptor antagonist **1** has been made on the basis of single-crystal X-ray diffraction data collected at a low temperature. The crystal structure of **1** consists of infinite ribbons in which molecules are connected by an N–H···N hydrogen bond and several interactions of the C–H···O, C–H···N, and C–H···S type. The molecular conformation, characterized by the *syn* orientation of a tetrazole and a pyrimidinone ring with respect to a phenyl spacer group, is stabilized by two short S···O and S···N intramolecular contacts between a substituted thiophene fragment and the other two heterocycles of **1**. The electrostatic nature of these interactions is documented. Furthermore, the Laplacian of $\rho(\boldsymbol{r})$ in the plane defined by the sulfur, oxygen, and nitrogen atoms involved in these interactions shows their strongly directional character as the regions of charge concentration on the valence shell of the nitrogen and oxygen atoms directly face the regions of charge depletion on the valence shell of the sulfur atom. All the chemical bonds and the relevant intra- and intermolecular interactions of **1** have been quantitatively described by the topological analysis of $\rho(\boldsymbol{r})$. Simple relationships between the bond path lengths (R_b) and the values of ρ at the bond critical points (ρ_{bcp}) have been obtained for the 28 C–C bonds, the seven N–C bonds, and the four O–C bonds. For the first two classes of bonds the relationship is in the form of a straight line, whose parameters, for the C–C bonds, agree, within experimental uncertainty, with those previously derived in our laboratory from a 19 K X-ray diffraction study of crystals of a different compound. Maps of the molecular electrostatic potential $\phi(\boldsymbol{r})$ derived from the experimental charge density display features that are important for the drug-receptor recognition of **1**.

Keywords: charge-density distribution · electrostatic interactions · interaction directionality · topological analysis · X-ray diffraction

Introduction

Molecules acting as receptor antagonists are particularly suited for studies aimed at determining the relationships between chemical properties and the biological activity of drugs. As, in general, their action does not involve metabolic processes, their molecular conformation and charge distribution are the true key features that govern drug-receptor recognition and all related intra- and intermolecular interactions. Therefore, a structural investigation of these molecules, including a detailed topological analysis of their electron-density distribution $\rho(\boldsymbol{r})$ in the solid state, can reveal fundamental insights, such as the relevance of directionality for some crucial interactions, as well as the relationships between charge density and geometrical parameters.

The present paper reports the case of a receptor antagonist of the hormone angiotensin II (AII), an octapeptide of sequence Asp-Arg-Val-Tyr-Ile-His-Pro-Phe, which is the biologically active component of the renin–angiotensin system (RAS) and which participates in a number of physiological functions associated with the regulation of blood pressure and fluid balance.[1] Drugs that inhibit the RAS have been shown to be effective in treating human hypertension. Over the last few years, AII nonpeptide receptor antagonists have

[a] Prof. R. Destro, Dr. L. Lo Presti
Dipartimento di Chimica Fisica ed Elettrochimica
Universita' di Milano, Via Golgi 19, 20133 Milano (Italy)
Fax: (+39) 02-503-14300
E-mail: riccardo.destro@unimi.it

[b] Dr. R. Soave, Dr. M. Barzaghi
CNR-ISTM, Istituto di Scienze e Tecnologie Molecolari
Via Golgi 19, 20133 Milano (Italy)

Supporting information for this article is available on the WWW under http://www.chemeurj.org/ or from the author.

 DOI: 10.1002/chem.200400964

proved to be a suitable alternative to inhibitors of angiotensin-converting enzyme (ACE) and renin in order to influence the RAS. In particular, the discovery,[2] by the DuPont group, of a series of *N*-(biphenylylmethyl)imidazoles as potent and orally active AII receptor antagonists has furthered progress in the area and stimulated a profusion of synthetic,[1a,3] spectroscopic,[4] and computational[5] research.

A series[6] of such AII antagonists contains a pyrimidinone ring which bears a carbon-linked biphenyltetrazole moiety and a carboxyheteroaryl group at the 3-position. By comparative analysis of the theoretical molecular electrostatic potential $\phi(\boldsymbol{r})$ in active and inactive compounds of the series, together with overlay studies employing a computational model of an AII active conformation, it was found that the compound named LR-B/081, that is, 2-[(4-butyl-2-methyl-6-oxo-5-{[2′-(1*H*-tetrazol-5-yl)-1,1′-biphenyl-4-yl]methyl}-6*H*-pyrimidin-1-yl)methyl]-3-thiophenecarboxylic acid, methyl ester (**1**), was one of the most effective in the series[6]. Therefore, it was selected as a candidate for further studies.[7–12] Its crystal structure was also determined by X-ray diffraction at room temperature.[13]

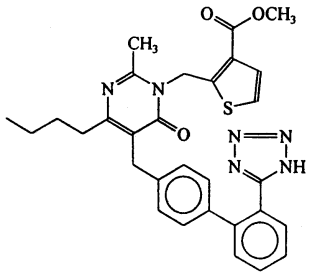

To gain an insight into the electrostatic requirements for LR-B/081 activity, a preliminary study of its experimental $\phi(\boldsymbol{r})$ was performed in our laboratory, and a comparison with theoretical results at the HF level has been recently published.[14] We report now the results of an X-ray investigation of $\rho(\boldsymbol{r})$ in LR-B/081 at $T=$ 17 K,[15] together with a quantitative description of all the covalent bonds and the main intra- and intermolecular interactions, in terms of a charge-density analysis using Bader's quantum theory of atoms-in-molecules (AIM).[16] The characterization of the electronic structure of this relatively large molecule, with five different rings and a wide range of chemical bonds (C–C, N–C, O–C, S–C, N–N, C–H, and N–H bonds plus interactions of the NH···N, CH···X (X = O,S,N), S···O, and S···N type), is a fitting case for exploiting the broad interpretive power of the AIM approach. Therefore, after a detailed discussion of the molecular conformation and the crystal packing, the results of an accurate topological analysis of $\rho(\boldsymbol{r})_{exp}$ are presented. A report on our latest investigation of the experimental electrostatic potential $\phi(\boldsymbol{r})$ follows, while the evaluation of molecular multipole moments and intermolecular interaction energies, currently in progress, will be reported separately.

To reduce the chances that artefacts, rather than genuine features of $\rho(\boldsymbol{r})$, be described, high-quality X-ray data measured at the lowest possible temperature are essential.[17] We have collected the diffracted intensities with a diffractometer equipped with a closed-cycle helium refrigerator and processed them with great and special care. Some decisive steps in the acquisition and treatment of data are described in detail in the Experimental Section. We emphasize here one feature of the model that we have adopted to analyze the measured X-ray intensities, that is, the anisotropic vibrational motion of the hydrogen nuclei. Indeed, as hydrogen atoms are critical for both the molecular electrostatic properties and the chemical reactivity,[18,19] accuracy in their positional and displacement parameters is crucial in electron-density studies of molecular crystals.

Results and Discussion

Effects of very low temperature: On going from room temperature (RT) to 17 K, a marked reduction in the thermal motion is observed, with atomic vibrational root-mean-square (rms) amplitudes about 30% as large at 17 K as they are at RT (Table 1). This reduction is much more pronounced than that observed in crystals in which the packing is dictated by strong hydrogen bonds, as, for instance, in the case of glycine,[20] whose rms vibrational amplitudes at 23 K

Table 1. Root-mean-square amplitudes Δr_{rms} of the atomic motion[a] and VALRAY[41] atomic charges.[b]

Atom	Δr_{rms}(296 K) [Å]	Δr_{rms}(17 K) [Å]	q [e]	Atom	Δr_{rms}(296 K) [Å]	Δr_{rms}(17 K) [Å]	q [e]
S1	0.2606	0.0746	+0.16(3)	C12	0.2445	0.0806	−0.14(5)
O1	0.2638	0.0816	−0.17(3)	C13	0.2456	0.0720	−0.16(4)
O2	0.2907	0.0843	−0.15(2)	C14	0.2152	0.0689	+0.03(4)
O3	0.3330	0.1016	−0.18(2)	C15	0.2202	0.0745	−0.12(4)
N1	0.2128	0.0687	−0.10(3)	C16	0.2360	0.0747	−0.10(4)
N2	0.2071	0.0638	−0.05(3)	C17	0.2163	0.0688	−0.01(4)
N3	0.2722	0.0817	−0.08(3)	C18	0.2470	0.0771	−0.05(5)
N4	0.2778	0.0834	−0.10(2)	C19	0.2496	0.0763	−0.04(4)
N5	0.2516	0.0793	−0.06(2)	C20	0.2460	0.0698	−0.01(4)
N6	0.2296	0.0741	−0.06(3)	C21	0.2827	0.0820	−0.03(5)
C1	0.2071	0.0667	−0.07(4)	C22	0.3225	0.0901	−0.06(5)
C2	0.2074	0.0669	−0.00(3)	C23	0.3347	0.0918	−0.09(5)
C3	0.2315	0.0670	+0.05(4)	C24	0.3066	0.0842	+0.03(5)
C4	0.2119	0.0670	−0.08(4)	C25	0.2443	0.0714	−0.06(4)
C5	0.2149	0.0705	−0.11(4)	C26	0.2229	0.0703	−0.02(3)
C6	0.2054	0.0703	−0.07(3)	C27	0.2398	0.0740	+0.01(5)
C7	0.2168	0.0724	−0.04(4)	C28	0.2983	0.0815	−0.01(4)
C8	0.2508	0.0812	−0.02(5)	C29	0.3025	0.0908	+0.01(5)
C9	0.2640	0.0840	−0.15(4)	C30	0.4044	0.0995	−0.10(5)
C10	0.2494	0.0766	+0.04(4)	⟨H⟩	0.32(7)	0.17(2)	+0.07(5)
C11	0.3225	0.0985	+0.06(5)				

[a] su of ~0.003 at 296 K and of ~0.0005 at 17 K. [b] su are given in parentheses.

are, on average, 46% as large as those at RT. We note that, when the temperature of the LR-B/081 crystal was lowered only to 120 K[21] (a temperature at which electron-density studies are sometimes performed), the rms amplitudes of the atomic motion were, on average, 58% as large as those at RT, hence almost twice as large as those at 17 K. It is well known that the largest feasible reduction in thermal motion must be pursued for an accurate deconvolution of the thermal motion from the static electron density. In particular, our results confirm an earlier anticipation by Stewart[22] that at a temperature as low as 17 K the correlations between positional and dipole parameters as well as those between anisotropic atomic displacement parameters (ADPs) and quadrupole parameters are not a serious problem, even if data are collected only up to $2\theta = 75°$ with $Mo_{K\alpha}$ radiation (as in the present experiment), rather than up to a higher resolution, for example, $2\theta_{max} = 109°$, as in some of our previous work[20,23] (see the Experimental Section for further details of the correlation coefficients). Moreover, we observe that the disorder in the terminal portion of the butyl chain of **1**, a disturbing feature of the room-temperature structure,[13] is no longer present at 17 K.

Geometry and molecular conformation: An ORTEP[24] plot of LR-B/081 is shown in Figure 1. The geometrical parameters of **1** obtained at 17 K are ten times more precise than those at room temperature, with standard uncertainties (su) < 0.001 Å for bond distances, $< 0.03°$ for bond angles, and $< 0.1°$ for torsion angles when only non-hydrogen atoms are implied. The lengths of the 12 C–C bonds of the two phenyl groups are in the range 1.3923(5)–1.4107(5) Å, with an average value (1.399 Å) much closer to that obtained[25] in a neutron study of benzene at 15 K (1.3983(7) Å) than to the average in the 40 K neutron study[26a] of biphenyl itself (1.410(9) Å). Furthermore, our resulting average C_{arom}–H bond length (1.079(10) Å) coincides, within 1 su, with that reported[27] as the average for 218 neutron-diffraction determinations of the C_{arom}–H bond distance (1.083(11) Å).

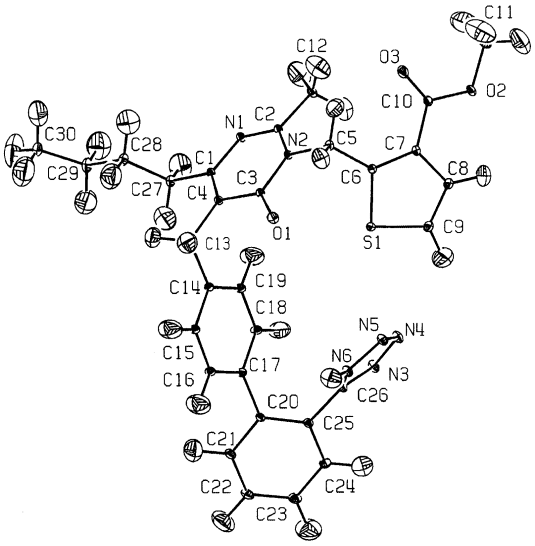

Figure 1. ORTEP plot of LR-B/081 at 17 K with the atom-numbering scheme. Hydrogen atoms are numbered according to the heavy atom to which they are bonded. Ellipsoids at 70% probability level.

The molecule of **1** has five different rings, a thiophene (R1), a pyrimidinone (R2), two phenyls (one (R3) *para* and one (R4) *ortho* substituted) and a tetrazole (R5). Rings R1, R3, R4, and R5 are almost perfectly planar, with maximum rms deviations of the ring atoms from their planes never exceeding 0.007 Å for rings R1, R3, and R5 and amounting to 0.017 Å (for atom C20) in ring R4. The six-membered ring of the pyrimidinone system assumes a half-boat conformation with puckering parameters[28] $Q = 0.043$ Å, $\theta = 50.5°$, and $\varphi = 59.6°$ for the atom sequence N2–C2–N1–C1–C4–C3. In this ring, the C3 atom is 0.0604(6) Å from the mean plane defined by the other five atoms, whose rms deviation from the plane is 0.002 Å.

The molecular conformation of LR-B/081 in the solid state is described by the torsion angles listed in Table 2. The relative orientation of the rings in the biphenyltetrazole (BPT) moiety is of particular note as this fragment has attracted special attention in molecular modeling[3c] as well as in spectroscopic and conformational analysis studies[5c] of peptidomimetic antagonists of AII. A search for the BPT system in the Cambridge Structural Database[29] (CSD, Version 5.24 of November 2002, with 272000 entries) identified a total of 12 different crystal structures, all of drugs of the same class as LR-B/081. For all but one structure, for which $\tau_2 = 64°$, the dihedral angle between the phenyl rings is in the range 41.7–51.3°, with an average value of 46(3)°. This value is the same, within experimental uncertainty, as that measured in the gas phase[26b] for normal and deuterated biphenyl, 44.4(1.2) and 45.5(1.6)°, respectively, the latter value being identical to that obtained by optimization of the molecular geometry of biphenyl at the HF/6-31G** level.[26c]

Table 2. Conformational parameters for LR-B/081 at 17 K.

Parameter	Torsion angle [°]
τ_1 = C20-C25-C26-N6	55.99(5)
τ_2 = C21-C20-C17-C16	50.84(4)
τ_3 = C15-C14-C13-C4	163.01(2)
τ_4 = C14-C13-C4-C3	−78.25(5)
τ_5 = C3-N2-C5-C6	92.44(3)
τ_6 = N2-C5-C6-C7	133.33(4)
τ_7 = C5-C6-C7-C10	−3.03(4)
τ_8 = C6-C7-C10-O2	−171.07(3)
τ_9 = C7-C10-O2-C11	176.57(3)
ϕ_1 = C4-C1-C27-C28	83.66(4)
ϕ_2 = C1-C27-C28-C29	173.08(2)
ϕ_3 = C27-C28-C29-C30	173.99(3)

For τ_1, the dihedral angle between the tetrazole ring and its adjacent phenyl ring, two values $< 40°$ are observed: 28.1° in the crystal form B of irbesartan[30] and 37.4° in the drug named CS-866.[3c] Apart from a value as large as 78.2° in a thiadiazoline derivative[3b] (refcode SIPSOZ in the CSD), all other eight values are clustered between 52.5 and

58.8°, although the low energy barrier for rotation around the bond connecting the two rings (~1.5 kcal mol^{-1})[5c] would allow an almost free rotation, and hence a possible larger range of values in the crystal structures. Evidently, similar electrostatic and/or packing forces, especially intermolecular hydrogen bonds, are responsible for the observed narrow range. Indeed, changes in the molecular environment usually lead to variations in the observed or predicted molecular conformation: see, for example, the case of losartan potassium, a prototypical compound for this class of drugs, originally named DUP753,[2] and its different conformations, as determined by NMR spectroscopy,[5c] molecular modeling,[5c] and X-ray crystal structure.[31]

For LR-B/081 the values of the torsion angles τ_1, τ_2, and τ_3 (Table 2) imply a *syn* orientation of the tetrazole and pyrimidinone rings relative to the 1,4-substituted phenyl ring. We note that such a conformation is stabilized by three relatively short intramolecular contacts: N4···H9, 2.751(6) Å; S1···N5, 3.2950(3) Å; S1···O1, 3.1995(3) Å. The electrostatic nature of the S···N interaction is suggested by the value of the charges of the two atoms, $+0.16(3)e$ for atom S1 and $-0.06(2)e$ for atom N5 (Table 1). Even stronger is the S1···O1 interaction, with a contact distance about 0.1 Å shorter than the sum of the van der Waals (vdW) radii (1.80 Å for sulfur, 1.70 Å for carbon, 1.55 Å for nitrogen, 1.52 Å for oxygen, and 1.20 Å for hydrogen).[32] Here too the electrostatic nature of the interaction is evident, the charge of the O1 atom being $-0.17(3)e$ (Table 1), as determined from the multipolar refinement of the X-ray data. The role of intramolecular nonbonded S···O interactions in the conformation and activity of biologically important systems has been investigated in the case of 1,4-type interactions,[33] while more recently X-ray crystallographic analyses and ab initio molecular orbital calculations have been used to specifically address the possible relevance of the 1,5-type S···O close contacts to the activity of AII receptor antagonists and related compounds.[3b] In the present molecule the interaction is of the 1,6 type, and the S···O distance is much longer than in the case of the 1,5-type contacts mentioned above, but it can be speculated that the concept of mimic-fused heterocycles[3b] might apply also to **1**.

The position of atom S1 with respect to atoms O1 and N5 is governed by the torsion angle τ_6, whose value, together with that of τ_8 (Table 2), brings atom O3 into proximity with atom H5A. The separation between the two atoms in this 1,6-type O···H close contact is as short as 2.200(6) Å.

Crystal packing: The basic crystal-packing pattern of LR-B/081 is illustrated by the partial view, down the *b* axis, shown in Figure 2. Two parallel, infinite ribbons, each formed by pairs of molecules related to each other by a crystallographic glide plane, run along the *c* axis. The molecules within each ribbon are connected by a NH···N hydrogen bond and several relatively short contacts of the CH···S, CH···O, and CH···N type. Interactions of the latter two types are observed between contiguous ribbons. We defer to a later section the discussion on whether such contacts can be classified as true hydrogen bonds[34] because we believe that the topological descriptors of $\rho(\boldsymbol{r})$, and not only the geometrical parameters, should be considered.

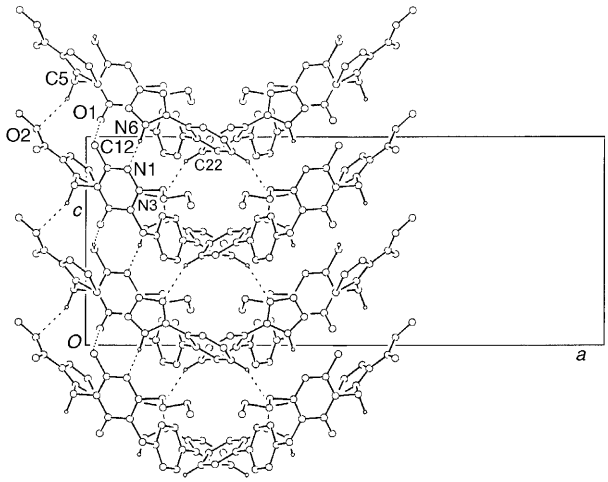

Figure 2. ORTEP drawing of two molecular stacks viewed down the *b* axis. Only those hydrogen atoms involved in intermolecular interactions (dashed lines) are shown.

The NH···N hydrogen bond connects the N6 atom of the tetrazole ring of one molecule to the N1 atom (the acceptor) of the pyrimidinone cycle of the other molecule of each pair. Owing to the geometry of the resulting fragment this hydrogen bond is classified as moderate (or normal) according to Jeffrey's categorization.[34a] Indeed, the values of the two N···N and H···N distances and that of the NH···N angle (see Table 5) are well within the range found in organic crystals in an earlier CSD search[35] on more than 280 selected crystal structures. More recently, an intermolecular NH···N hydrogen bond very similar to that of LR-B/081 was observed[36] between the tetrazole and the other heterocycle in a BPT imidazo[4,5-*b*]pyridine-based AII receptor antagonist (refcode ZUHTEB in CSD) and the same kind of hydrogen bond is also present in the crystal packing of histidine,[19] one of the components of the AII hormone. The importance of the presence of an aromatic nitrogen atom functioning as a hydrogen bond acceptor in the LR-B/081 class of drugs has been recently stressed in a study of pharmacophore models.[5a]

Electron-density deformation maps: The important features of electron distribution in crystals may be displayed in various kinds of difference-density maps.[37] Examples of such maps for the tetrazole and thiophene fragments of LR-B/081 are shown in Figures 3 and 4, respectively. However, although appealing for their pictorial effectiveness and visual conciseness, such dynamic or static deformation maps may suffer from serious shortcomings, such as a dependence on data resolution (compare Figure 3a and 3b) or scale factors,[38] as well as on the radial parameters adopted in the multipole model. This hampers any quantitative comparison between results from different investigations if precise values for the positions of the $\Delta\rho(\boldsymbol{r})$ peaks and their heights

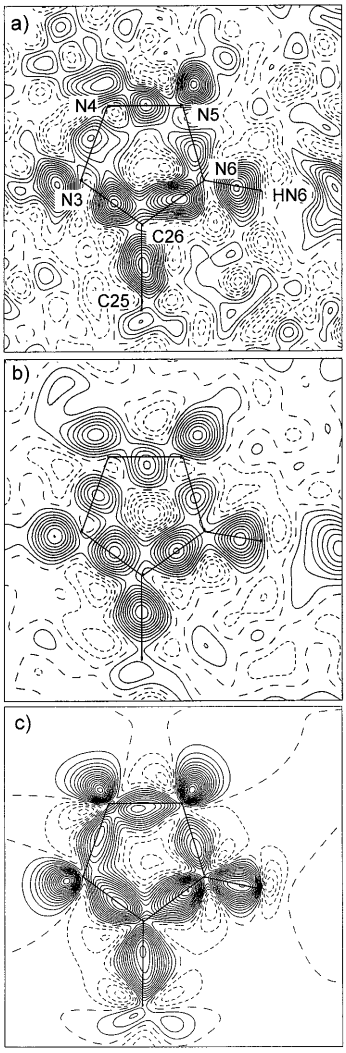

Figure 3. Contour maps of $\Delta\rho$ in the plane of the tetrazole ring of LR-B/081 (6 Å × 6 Å; plane defined by atoms N4 and N6 and the point at $^1/_4$ of the distance between atoms N6 and N3). Contours are plotted at intervals of 0.05 e Å^{-3} units. Solid lines show the positive regions of $\Delta\rho$, dashed lines the negative regions. a) Dynamic deformation density from all data; b) dynamic deformation density from data within $\sin\theta/\lambda = 0.65$ Å^{-1}; c) static deformation density from all data.

are sought. Hence, we believe that only a qualitative comparison is appropriate, for instance, between our dynamic deformation density of Figure 3b and that reported[39] for the tetrazole ring in a polypeptide studied at $T = 125$ K with data within $(\sin\theta/\lambda) = 0.65$ Å^{-1}, the two maps showing some similarities and several differences. On the other hand, the static maps of Figures 3c and 4 clearly illustrate how different the deformation of $\rho(\boldsymbol{r})$ is, upon bonding, for the various individual atomic components of the two heterocycles. Yet a full and quantitative characterization of the interatomic interactions cannot be derived from such maps and is obtained only through a topological analysis of the total $\rho(\boldsymbol{r})$, as reported for LR-B/081 in the following section.

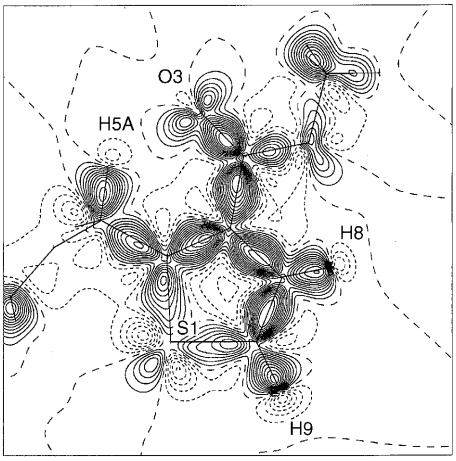

Figure 4. Contour map of the static deformation density $\Delta\rho$ in the plane of the thiophene ring of LR-B/081 (9 Å × 9 Å; the plane is defined by atoms C6, C7, and C9). Contours and units as in Figure 3.

Topological properties of $\rho(\boldsymbol{r})$: Experimental electron distributions can be analyzed in terms of their topological features,[17,40] as theoretical charge distributions are, following Bader's AIM theory.[16] Of the critical points (points at which $\nabla\rho = 0$), special attention is given to those called bond critical points (bcps), which occur on a line of maximum charge density with respect to any lateral displacement and link two nuclei (bond path). Beyond the number and kind of critical points, other topological indicators often used to describe $\rho(\boldsymbol{r})$ are as follows:

1) the value of ρ_{bcp};
2) those of the principal curvatures of ρ, usually called λ_1, λ_2, and λ_3;
3) the corresponding value of the Laplacian $\nabla^2\rho = \lambda_1 + \lambda_2 + \lambda_3$;
4) the bond ellipticity $\varepsilon = (\lambda_1/\lambda_2) - 1$;
5) the bonded radius R_X, which is the distance along the bond path from the bcp to one of the two bonded nuclei.

Table 3 reports most of the properties of the bcps for all the covalent bonds of LR-B/081, while a full list can be found in the Supporting Information. The properties of eight ring critical points (rcps) are reported in Table 4, while those of the most relevant intra- and intermolecular contacts are listed in Table 5.

The critical points of the density were searched by using a Newton–Raphson algorithm implemented in the VALRAY code[41] starting from a suitable initial guess of their positions. A set of 78 bcps was searched and found, including all the 74 conventional covalent bonds of the molecule (Table 3), together with the four intramolecular contacts (see Table 5) described above (N4···H9, S1···N5, S1···O1, and O3···H5A). The bond path lengths (R_b, see the Supporting Information) and the standard uncertainties of both the curvatures and the ε values were evaluated with the PAMoC code.[42]

Table 3. Topological properties of the bond critical points of LR-B/081.

Bond	R_e[a] [Å]	R_X/R_b[b]	ρ_{bcp} [e Å^{-3}]	$\nabla^2\rho_{bcp}$ [e Å^{-5}]	λ_3 [e Å^{-5}]	ε[c]
C2–C12	1.4933(5)	0.524	1.80(2)	−14.1(9)	11.0(6)	0.03(7)
C5–C6	1.5029(4)	0.487	1.70(2)	−12.4(8)	10.9(6)	0.08(5)
C4–C13	1.5032(4)	0.501	1.75(2)	−13.3(8)	11.0(5)	0.09(5)
C13–C14	1.5193(4)	0.487	1.61(2)	−10.0(8)	11.0(5)	0.14(8)
C1–C27	1.5061(4)	0.525	1.74(2)	−13.3(8)	10.9(4)	0.02(5)
C27–C28	1.5365(5)	0.511	1.60(2)	−10.4(8)	10.9(2)	0.06(4)
C28–C29	1.5305(5)	0.496	1.63(2)	−10.3(8)	11.3(2)	0.04(4)
C29–C30	1.5270(5)	0.491	1.60(2)	−10.2(8)	10.9(4)	0.06(9)
C14–C15	1.3996(5)	0.476	2.12(3)	−19(1)	10.5(5)	0.18(5)
C14–C19	1.3966(5)	0.495	2.13(2)	−19.5(9)	10.6(7)	0.16(7)
C15–C16	1.3958(5)	0.500	2.09(3)	−17.9(9)	11.1(7)	0.2(1)
C16–C17	1.4026(5)	0.505	2.07(2)	−17.4(9)	11.0(7)	0.13(8)
C17–C18	1.4006(5)	0.497	2.06(2)	−17.2(9)	11.0(6)	0.20(5)
C18–C19	1.3921(5)	0.529	2.14(3)	−19(1)	10.4(7)	0.21(8)
C20–C21	1.4014(4)	0.500	2.14(2)	−18.6(9)	11.2(5)	0.23(9)
C20–C25	1.4109(5)	0.504	2.04(2)	−17.2(9)	10.9(7)	0.22(7)
C21–C22	1.3962(5)	0.496	2.15(3)	−19.6(9)	10.9(2)	0.17(4)
C22–C23	1.3969(5)	0.486	2.14(3)	−20(1)	10.8(8)	0.12(9)
C23–C24	1.3930(5)	0.511	2.16(3)	−19(1)	11.1(5)	0.20(9)
C24–C25	1.3986(5)	0.470	2.10(3)	−18(1)	10.6(6)	0.2(1)
C17–C20	1.4829(4)	0.496	1.79(2)	−14.0(8)	11.0(5)	0.2(1)
C7–C10	1.4779(5)	0.473	1.87(2)	−15.1(9)	11.3(3)	0.15(4)
C25–C26	1.4725(4)	0.491	1.91(2)	−15.4(8)	11.6(5)	0.03(9)
C3–C4	1.4440(4)	0.500	2.00(2)	−16.7(9)	11.5(6)	0.16(8)
C1–C4	1.3698(4)	0.511	2.20(2)	−19(1)	10.8(7)	0.24(9)
C7–C8	1.4330(5)	0.490	2.05(2)	−18.7(9)	10.9(7)	0.22(7)
C6–C7	1.3824(4)	0.479	2.13(3)	−17(1)	10.9(5)	0.23(8)
C8–C9	1.3660(5)	0.487	2.25(3)	−21(1)	10.7(7)	0.30(7)
N2–C5	1.4749(4)	0.581	1.70(3)	−11(1)	12.4(6)	0.03(7)
N2–C3	1.4069(4)	0.582	2.09(3)	−22(2)	11.7(6)	0.13(5)
N1–C1	1.3852(4)	0.560	2.18(3)	−19(1)	14.2(6)	0.10(4)
N2–C2	1.3669(4)	0.593	2.25(4)	−25(2)	10.8(9)	0.12(6)
N6–C26	1.3444(4)	0.635	2.31(5)	−27(3)	9(1)	0.10(6)
N3–C26	1.3287(5)	0.576	2.49(4)	−28(2)	12.1(8)	0.19(4)
N1–C2	1.3154(4)	0.586	2.51(4)	−26(2)	12(1)	0.19(8)
O2–C11	1.4409(5)	0.590	1.66(3)	−9(2)	13.9(7)	0.16(9)
O2–C10	1.3475(5)	0.614	2.16(4)	−24(2)	11(1)	0.20(7)
O1–C3	1.2320(4)	0.641	2.79(5)	−30(4)	20(2)	0.16(4)
O3–C10	1.2178(5)	0.658	2.85(6)	−19(5)	33(2)	0.09(8)
S1–C6	1.7216(3)	0.506	1.40(2)	−4.5(5)	9.4(3)	0.2(1)
S1–C9	1.7208(3)	0.512	1.40(2)	−5.3(5)	9.4(3)	0.2(1)
N4–N5	1.2982(5)	0.503	2.83(3)	−13(2)	34(1)	0.09(6)
N5–N6	1.3465(5)	0.492	2.53(3)	−8(1)	32.5(9)	0.10(6)
N3–N4	1.3602(5)	0.496	2.52(3)	−9(1)	33.0(9)	0.05(5)
N6–HN6	1.029(16)	0.744	2.23(6)	−45(5)	21(2)	0.01(5)
⟨C–H⟩[d]	1.082(14)	0.609	1.90(6)	−19(2)	15(1)	0.06(4)

[a] Experimental bond lengths are uncorrected for thermal motion. [b] R_X = distance from the first atom of the pair to the critical point (su of about 0.002 Å). R_b = bond path length. R_X and R_b are measured in Å. [c] Ellipticity, defined as $(\lambda_1/\lambda_2)-1$. [d] In view of the essential identity, in chemical terms, of the 29 C–H bonds, their bcp values are reported as averages, while those of the unique N–H bond are shown separately.

C–C bonds: As expected, the bcps are located very close to the midpoint of the C–C bonds ($\langle R_X/R_b\rangle = 0.50(1)$). A plot of ρ_{bcp} (e Å^{-3}) versus the bond path length R_b (Å) for the 28 C–C bonds of LR-B/081 is shown in Figure 5 (top). As in the case of citrinin,[23c] the dependence of ρ_{bcp} on R_b can be adequately represented by a straight line, given here by Equation (1), with a correlation coefficient of −0.984. The slope and intercept values coincide, within experimental error, with those of the straight line for citrinin (−3.8 and 7.4, respectively), while the correlation coefficient (−0.996 in citrinin) is less satisfactory. Anyhow, for LR-B/081 the differences between the experimental ρ_{bcp} values and those calculated on the straight line never exceed 0.07 e Å^{-3} ($\leq$3.5 su).

$$\rho_{bcp} = -3.7(1)\cdot R_b + 7.3(2) \quad (1)$$

A well-defined trend is observed in the values of the bond ellipticity ε for the C–C bonds (Table 3): for the eight single bonds involving at least one sp^3 carbon atom the average value of ε is 0.06; for the three bonds with bond lengths in the range 1.472–1.483 Å, $\langle\varepsilon\rangle = 0.13$; for the 12 aromatic bonds in the two phenyl rings, $\langle\varepsilon\rangle = 0.19$; and for the remaining five bonds, which are all C(sp^2)–C(sp^2) bonds involved in conjugative interactions, $\langle\varepsilon\rangle = 0.23$. (In the latter group, the average ε becomes 0.26 if only the three shortest bonds, that is, those with the largest double-bond character, are considered.) These values reflect an increased contraction of the density towards the bond path with increasing bond order. The increase (in absolute value) of λ_1 dominates that of λ_2 and leads to the observed trend in the ellipticities: the density at the bcps of double bonds is more curved along the minor axis of the bond than at those of single bonds. Values of λ_3 are instead nearly constant for all the 28 C–C bonds of LR-B/081, lying in the very narrow range of 10.4–11.6 e Å^{-5}.

N–C bonds: A shift of the bcps towards the carbon nucleus is observed for all seven N–C bonds of the molecule, with

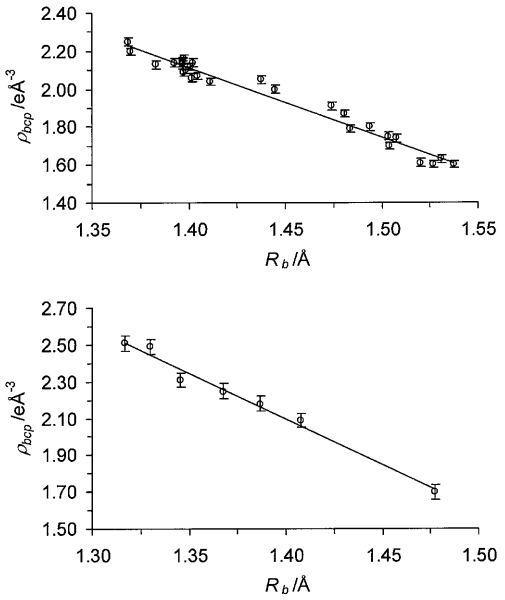

Figure 5. Values of the electron density (ρ_{bcp}) at the C–C (top) and the C–N (bottom) bond critical points versus the bond path lengths (R_b). The su of ρ_{bcp} are shown as vertical bars.

R_X/R_b ranging from 0.560 to 0.635. Equation (2) describes the least-squares straight line obtained for the plot of ρ_{bcp} versus R_b for the N–C bonds (Figure 5 bottom), which has a correlation coefficient of −0.993. The fit is considerably better than that obtained for the C–C bonds. Clearly, the differences in the slope and intercept values of Equations (1) and (2) are inherent to the different electronic natures of the carbon and nitrogen atoms.

$$\rho_{bcp} = -5.0(3) \cdot R_b + 9.1(4) \quad (2)$$

Six of the N–C bonds belong to ring fragments, and the values of their path lengths are uniformly spread between 1.315 and 1.407 Å. The remaining N–C bond, which is 1.475 Å long, is the only bond in **1** that connects a nitrogen atom to an sp^3 carbon atom. The overall, rather wide range of bond lengths is typical of systems with several N–C bonds involved in an extensively conjugated system, for example, as in the purine rings of 9-ethylguanine.[43]

The fit given by Equation (2) is better than that obtained[44] with a logarithmic relationship based on 11 calculated (at the B3LYP and MP2 level with the 6-311++G** basis set) pairs of ρ_{bcp} and R_b values. Indeed, from Equation (2) the largest difference between the calculated and observed ρ_{bcp} values is 0.04 e Å^{-3}, while the logarithmic Equation (3)[44] would give differences of 0.16 and 0.21 e Å^{-3} for the two shortest N–C bonds. We note also that Equation (2) is in only modest, qualitative agreement with the ρ_{bcp} versus R_b relationship recently reported for HF/3-21G-calculated ρ_{bcp} values of the 46 C–N bonds (bond lengths in the range 1.30–1.36 Å) in the protein crambin (slope = −4.0836, intercept = 7.5476).[45]

$$\ln \rho_{bcp} = 1.809 - 2.183 \cdot R_b \quad (3)$$

A much larger range of λ_3 values is observed for the N–C bonds than for the C–C bonds; the values of the positive curvature observed for the N–C bonds vary between 9 e Å^{-5} for the C26–N6 bond and 14 e Å^{-5} for the C1–N1 bond (average su < 1 e Å^{-5}). As expected, the absolute value of λ_1 increases while R_b decreases, that is, while the bond order increases.

O–C bonds: The average distance of the bcps from the oxygen atom in the two formal C=O bonds is $0.650R_b$, to be compared with an average value of $0.602R_b$ for the other two O–C bonds. The R_b and ρ_{bcp} values of the four O–C bonds of LR-B/081 satisfy moderately well the best correlation found for the six bonds of the same kind in citrinin,[23c] that is, by the exponential[46] given by Equation (4).

$$\rho_{bcp} = 8.443 \cdot R_b^{-3.521} \quad (4)$$

In compound **1**, the differences between the experimentally determined ρ_{bcp} values and those predicted by Equation (4) are within 3 su, the largest disagreement occurring at the C10–O3 bond, with an expected ρ_{bcp} of 3.03 e Å^{-3} compared with the observed value of 2.85(6) e Å^{-3}.[47]

S–C bonds: The topological indicators of these bonds are reported in the literature[48–53] to range from 1.03 to 1.45 e Å^{-3} for ρ_{bcp} and from −0.90 to −9.78 e Å^{-5} for $\nabla^2\rho_{bcp}$. In keeping with the aromaticity of the thiophene ring, the two S–C bonds of LR-B/081 (Table 3) are among the shortest of those analyzed topologically, with ρ_{bcp} and $\nabla^2\rho_{bcp}$ values (1.40 e Å^{-3} and −4.5 e Å^{-5} for the S1–C6 bond and 1.40 e Å^{-3} and −5.3 e Å^{-5} for the S1–C9 bond) very close to those of the two S–C bonds of similar length in the thiazole fragment of polymorphs A and B of the anti-ulcer drug famotidine.[53]

N–N bonds: The three N–N bonds present in the tetrazole ring of **1** provide insufficient data to establish a really meaningful relationship between the ρ_{bcp} and R_b values. The linear fit (ρ_{bcp} versus R_b) here gives Equation (5) with a rather poor correlation coefficient of −0.974. The high uncertainty in the values of the slope and intercept reflects the contradictory situation for the two longer bonds (see Table 3) which differ by 0.014 Å (more than 27 su) in length, but only by 0.01 e Å^{-3} (1 su) in the ρ_{bcp} values.

$$\rho_{bcp} = -5(1) \cdot R_b + 10(2) \quad (5)$$

The tetrazole ring: We are not aware of any reported, detailed topological study of this system, which appears as the elective acidic group in sartan drugs (see Chart 2 of ref. [5b]). In LR-B/081 the total charge of this fragment

amounts to $-0.15(7)e$, with a contribution of $-0.30(6)e$ from the four nitrogen atoms, all of which are negatively charged. The N4–N5 bond has the shortest bond length in the ring, the highest value of ρ_{bcp}, and the most negative value of $\nabla^2\rho_{bcp}$, although all three N–N bonds have high ρ_{bcp} values, which, together with the planar arrangement, are indicative of π delocalization. Quite surprisingly, these values are accompanied by low (in modulus) values of $\nabla^2\rho_{bcp}$ compared, for instance, with those of the ring's N–C bonds. Note also that the large value of ρ at the ring critical point ρ_{rcp} of the tetrazole fragment (Table 4) is far larger than that of the other four "conventional" rings, including thiophene, the other five-membered ring of LR-B/081.

Table 4. Topological properties at the ring critical points of LR-B/081.

Ring[a]	ρ_{rcp} [e Å^{-3}]	$\nabla^2\rho_{rcp}$ [e Å^{-5}]	d_{rcp}[b] [Å]
R1	0.311(9)	5.1(1)	0.020
R2	0.182(7)	3.63(7)	0.037
R3	0.187(7)	3.24(6)	0.001
R4	0.178(7)	3.26(6)	0.018
R5	0.52(1)	9.7(2)	0.006
R6	0.095(4)	1.44(2)	0.016
R7	0.038(1)	0.47(1)	0.044
R8	0.062(2)	0.77(1)	0.427

[a] R1: S1-C9-C8-C7-C6; R2: C1-N1-C2-N2-C3-C4; R3: C14-C15-C16-C17-C18-C19; R4: C20-C21-C22-C23-C24-C25; R5: C26-N3-N4-N5-N6; R6: O3-C10-C7-C6-C5-H5A; R7: S1-N5-N4-H9-C9; R8: O1-C3-N2-C5-C6-S1. [b] Distance of the ring critical point from the least-square plane of the ring.

The contour map of $-\nabla^2\rho$ in the plane of the tetrazole ring (Figure 6) clearly shows the lone-pair charge concentrations on the N3, N4, and N5 atoms, anticipating the overall pattern of the electrostatic potential in the same plane (see below).

Intramolecular short contacts: Table 5 lists the topological properties of four relevant intramolecular interactions in **1**.[54] The most interesting features of two of these interactions, S1···N5 and S1···O1, are shown in the maps of $\rho(\boldsymbol{r})$ and its negative Laplacian in the plane defined by the three S1, N5, and O1 atoms (Figure 7). The locations of the two saddle points are clearly indicated by the shapes of the contours at 0.05 and 0.0625 e Å^{-3} in Figure 7a, while Figure 7b illustrates the directionality of the two interactions, with regions of charge concentration on the nitrogen and oxygen atoms facing the regions of charge depletion in the valence shell of the S1 atom. The features of the intramolecular S···N contact in **1** resemble those reported[55] for a shorter (3.0882(8) Å) intermolecular contact in tetrasulfur tetranitride, S_4N_4, for which the topology of the experimental and theoretical charge densities revealed similar directional interactions. Owing to the longer separation, the value of ρ_{bcp} for this interaction in **1** is smaller than that in S_4N_4 (0.050(1) e Å^{-3} versus 0.085(1) e Å^{-3}).

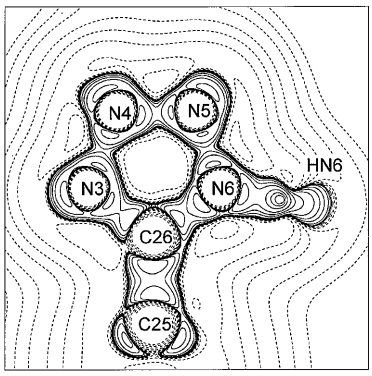

Figure 6. Contour map of $-\nabla^2\rho$ in the plane of the tetrazole ring (6 Å × 6 Å; plane defined by atoms N4 and N6 and the point at 1/4 of the distance between atoms N6 and N3). Contours are plotted at variable intervals in units of e Å^{-5}. Solid lines show the negative regions of $\nabla^2\rho$ (indicating charge concentration), dashed lines the positive regions (indicating charge depletion).

The H5A···O3 interaction results in the formation of the six-membered ring R6 of Table 4, with a C5–H5A···O3 angle of 126.3(4)° and a C10–O3···H5A angle of 102.1(2)°. The distance between the bcp on the H5A···O3 bond path and the ring critical point (rcp) of ring R6 is 0.577 Å. Although short, such a separation is large enough to exclude possible topological instability of the ring,[16] even if a close alignment (11.8°) between the major axis of the H5A···O3 bond and the eigenvector for λ_2 at the rcp is observed.

Similarly, the two interactions S1···N5 and H9···N4 lead to the five-membered ring R7 of Table 4. The five atoms of the ring are far from being coplanar, with atom N4 at 0.43 Å from the mean plane and atom N5 at 0.54 Å on the opposite side of the plane. The distances between the rcp of this ring and the bcps of these two short intramolecular contacts are 0.89 Å for S1···N5 and 0.68 Å for H9···N4. $\rho(\boldsymbol{r})$ at the rcp is flatter for R7 than for R6, and the eigenvector for λ_2 at the rcp of ring R7 is closely aligned with the major axis of the H9···N4 bond, at an angle of 6.8°. No appreciable alignment with the major axis of S1···N5 is observed, the corresponding angle being 27.2°.

The rcp of ring R8 (Table 4), that is, the ring created by the S1···O1 interaction, is only 0.24 Å from the bcp of this short intramolecular contact. Although small, such a distance indicates that the two critical points are still far from merging and annihilating each other through a fold catastrophe.[16]

Intermolecular interactions: Figure 8 shows the map of $-\nabla^2\rho(\boldsymbol{r})$ in the plane of the intermolecular N6–HN6···N1′ hydrogen bond. A marked polarization of the Laplacian of ρ around the hydrogen atom towards the acceptor atom N1′ can be observed. It has been noted[56,57] that such a feature, typical of some hydrogen bonds, can be seen only if multipole models for the hydrogen atoms include quadrupolar electron-density functions (which, in turn, can be adopted only if anisotropic ADPs for these atoms are taken into account). The bond path trajectory along NH···N is almost perfectly linear, with the N–H bond path only 0.001 Å longer than the corresponding internuclear distance and the H···N bond path identical to the atom–atom distance.

Table 5. Geometrical and topological properties of the most relevant intra- and intermolecular interactions.[a]

	Bond lengths [Å]			Bond angle [°]			
	D–H	H···A	D···A	D–H–A	ρ_{bcp}[b] [e Å^{-3}]	$\nabla^2\rho_{bcp}$[b] [e Å^{-5}]	R_X/R[c]
intramolecular interactions							
C5–H5A···O3	1.081(6)	2.200(6)	2.9710(5)	126.3(4)	0.120(8)	1.74(7)	0.406
C9–H9···N4	1.060(6)	2.751(6)	3.5142(5)	128.9(4)	0.043(3)	0.54(1)	0.421
S1···N5			3.2950(3)		0.050(1)	0.60(1)	0.530
S1···O1			3.1998(3)		0.063(2)	0.74(1)	0.532
intermolecular interactions							
N6–HN6···N1[d]	1.029(10)	1.871(10)	2.8972(5)	174.1(8)	0.310	0.97	0.359
C12–H12C···O1[e]	1.064(7)	2.345(7)	3.3733(5)	162.0(5)	0.067	0.92	0.403
C5–H5B···O2[d]	1.096(6)	2.460(6)	3.4873(5)	155.6(4)	0.069	0.82	0.409
C28–H28B···O2[f]	1.097(6)	2.743(6)	3.6500(5)	139.7(4)	0.033	0.48	0.411
C30–H30B···O3[f]	1.094(6)	2.994(6)	3.7392(5)	125.7(4)	0.022	0.30	0.450
C12–H12A···S1[e]	1.068(6)	3.068(6)	3.5941(3)	111.2(4)	0.043	0.50	0.407
C12–H12A···N5[e]	1.068(6)	2.329(6)	3.3894(5)	172.1(5)	0.087	1.05	0.391
C11–H11C···N3[g]	1.064(7)	2.508(7)	3.5601(6)	169.9(5)	0.067	0.71	0.419
C22–H22···N3[h]	1.079(6)	2.516(6)	3.4991(5)	151.0(5)	0.065	0.78	0.404
C12–H12B···N5[f]	1.077(6)	2.553(6)	3.5615(5)	155.6(4)	0.056	0.71	0.401
C5–H5A···N4[f]	1.081(6)	2.677(6)	3.4814(5)	130.9(4)	0.055	0.68	0.408
C9–H9···N2[i]	1.060(6)	2.941(6)	3.5850(5)	119.7(4)	0.031	0.42	0.431
C12–H12A···N6[e]	1.068(6)	2.608(6)	3.5046(5)	141.2(4)		no bcp	
C5–H5A···N5[f]	1.081(6)	2.630(6)	3.5879(5)	147.3(4)		no bcp	
C11–H11C···N4[g]	1.064(7)	2.634(7)	3.5099(6)	139.4(4)		no bcp	

[a] See also a full version of the table in the Supporting Information (Table S3). [b] At the bcp of the H···A/D···A interaction for DH···A/D···A contacts, respectively. For intermolecular interactions, there are su of 0.002–0.012 for ρ and 0.01–0.04 for $\nabla^2\rho$. [c] R_X = distance from the hydrogen/donor atom to the critical point of the H···A/D···A noncovalent bond (su of about 0.002 Å); R = bond length. [d] At (x, $^1/_2-y$, $-^1/_2+z$). [e] At (x, $^1/_2-y$, $^1/_2+z$). [f] At ($-x$, $^1/_2+y$, $^1/_2-z$). [g] At ($-x$, $-y$, $1-z$). [h] At ($^1/_2-x$, $-y$, $-^1/_2+z$). [i] At ($-x$, $y-^1/_2$, $^1/_2-z$).

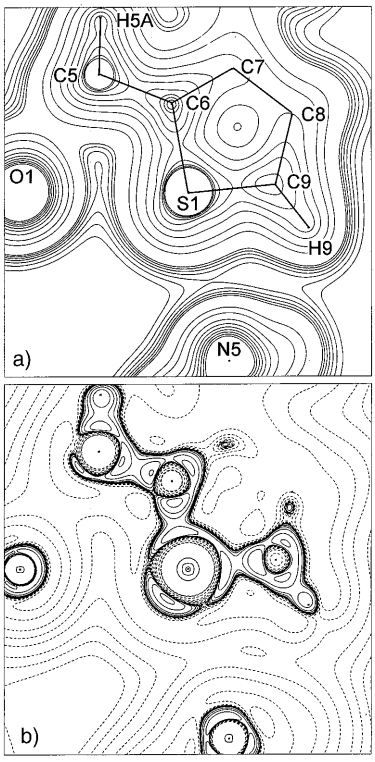

Figure 7. Contour maps (7 Å × 7 Å) of a) ρ and b) its negative Laplacian $-\nabla^2\rho$ in the plane defined by the S1, N5, and O1 atoms. a) The contour levels are at 0.025, 0.0375, 0.05, 0.0625, 0.075, 0.0875, 0.1, 0.4, 0.7, 1.0, 1.3, 1.6, 1.9, 2.2, and 2.5 e Å^{-3}. b) The contour levels and lines are as described in Figure 6.

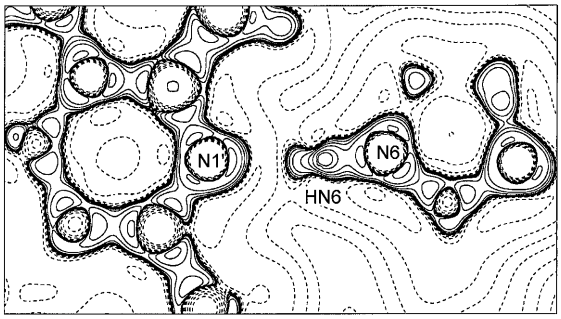

Figure 8. Contour maps of $-\nabla^2\rho$ in the plane of the intermolecular hydrogen bond N6–HN6···N1′ (9 Å × 5 Å; plane defined by atoms N1′ and HN6 and the bond critical point of the N1′···HN6 bond). Contour levels and lines are as described in Figure 6. Atom N1′ is the same as atom N1 of Table 5.

Besides the NH···N hydrogen bond, all the relevant intermolecular interactions of **1** are of the CH···X type, where X = O, S, or N (Table 5). The critical points of these interactions all share the same features of low values of ρ, which decrease as the interatomic separation increases, and of positive $\nabla^2\rho$ values, indicative of closed-shell interactions or ionic-type bonding. As usual in these cases, the Laplacian is dominated by the positive curvature along the internuclear line. We note that atom N5 is simultaneously engaged in three interactions and atom H12A in two (the shortest CH···N and the relatively long CH···S).

Of the interactions of the CH···X type, those where X = O are the most studied,[34c,58] and the relevance of weak CH···O hydrogen bonds in biological systems is well established. Recently, the role and properties of these bonds have been extensively studied by topological analysis of the bis-(dimethylamino) derivative of cyclobutene-1,2-dione (DMACB),[59] a system particularly suited for a thorough investigation of CH···O interactions because 23 unique CH···O short contacts are observed in its crystals (in which no other contacts closer than the sum of vdW radii are present). As in the case of DMACB, the bcps of all the H···O contacts in LR-B/081 less than 3.0 Å (four in number) were searched for and all four were found (Table 5). Both the geometrical and topological features of these CH···O interactions are well within the range of those, 19 out of 23, which, in the DMACB case, were classified as hydrogen bonds by the Koch and Popelier criteria.[60]

On topological grounds, six out of the nine CH···N intermolecular contacts reported in Table 5 would all be regarded as hydrogen bonds (including C9–H9···N2, with an H···N contact well above the sum of the vdW radii, 2.75 Å[32a]). We note that only one of them, C12–H12A···N5, satisfies Mascal's[32a] purely geometrical criteria for such a classification, as for this interaction the H···N distance is less than 2.45 Å and the CH···N angle is between 170 and 180°.

As for the remaining short interaction given in Table 5, that is C12–H12A···S1, it has been pointed out[34b] that hydrogen bonds of this kind have not yet been systematically investigated. In the present case, the long H···S separation and the small C–H···S angle would favour this contact to be classified as a short vdW interaction, although the recent literature[61] also classifies C–H···S interactions, in which the angle is in the range 105–118°, as possible hydrogen bonds. On the other hand, if the criterion that Koch and Popelier[60] consider as sufficient for the existence of a hydrogen bond is examined, one finds that there is a total mutual penetration between H12 and S1 of 0.75 Å. Hence, on this basis, even this interaction is to be considered a true hydrogen bond.

Electrostatic potential: It is well known that one of the most useful applications of charge densities is the derivation of the molecular electrostatic potential $\phi(\boldsymbol{r})$, which can be used as a highly sensitive measure to predict the strength of intermolecular interactions.[53] Owing to the geometric and electrostatic complementarity between a drug and its receptor, the knowledge of $\phi(\boldsymbol{r})$ can give novel insights into electronic receptor environments in drug–receptor molecular recognition processes.[62] The electrostatic potential of **1** in the crystal state has been obtained from the refined multipolar parameters following the procedure of Stewart.[63] Maps of the potential associated with some relevant molecular fragments removed from the crystal are shown in Figure 9. The essential features of these maps confirm the findings of the preliminary[14] study of $\phi(\boldsymbol{r})$ in **1** when the multipolar model for the interpretation of X-ray data was not as complete as that adopted here. In particular, Figure 9a and 9c show two regions of negative potential around the N1 and O1 atoms of

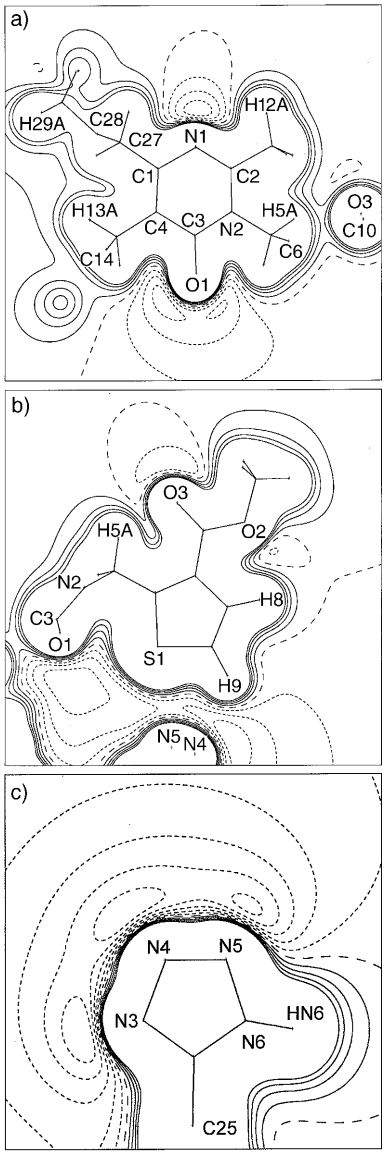

Figure 9. Contour maps of $\phi(\boldsymbol{r})$ in some relevant planes of LR-B/081. a) Pyrimidinone ring (12 Å × 12 Å; plane defined by the C1, C4, and N2 atoms); b) thiophene ring (12 Å × 12 Å; plane defined by atoms C6, C7, and C9); c) tetrazole ring (8 Å × 8 Å; plane defined by atoms N4 and N6 and the point at $^1/_4$ of the distance between atoms N6 and N3). Contours are plotted at intervals of 0.03 e Å^{-1} (1 e Å^{-1} ≡ 332.1 kcal mol^{-1}). Negative and zero contours: short and long dashed lines, respectively; positive contours: solid lines.

the pyrimidinone moiety (in Figure 9a, minima of −37 and −36 kcal mol^{-1}, respectively), and one, also negative, split into three relative minima surrounding the outermost part of the acidic tetrazole ring (−60 kcal mol^{-1} near atom N3, −58 kcal mol^{-1} near atom N4, and −53 kcal mol^{-1} near atom N5, Figure 9c).[64] The $\phi(\boldsymbol{r})$ distribution in the plane of the thiophene ring, as obtained by including the contribution of all atoms of **1** (Figure 9b), shows two rather shallow minima close to the two electronegative oxygen atoms (−17 kcal mol^{-1} at 1.317 Å from atom O3 and −12 kcal mol^{-1} at 1.315 Å from atom O2) separated from an

electropositive region around the methyl group. As seen in the lower part of the map, the minima of the pyrimidinone (on the left) and of the tetrazole (on the right) merge to form a unique wide, negative region markedly modified by the interplay of the potential around the thiophene ring.

In agreement with previous computational findings,[5d,6,14] it appears that the features of $\phi(\boldsymbol{r})$ that play a key role in the binding to the AII receptor are the strongly electrophile-attractive regions bulging out from the central heterocycle −N= type nitrogen atom and from the lactamic oxygen atom, and a region of positive long-range potential around the 6-butyl chain, the latter being believed to fit into a lipophilic pocket of the receptor that accommodates the Ile^5 side chain of AII.[2] It has to be stressed that while all these key features clearly emerge from the maps reported here (obtained from the refined multipolar parameters up to the hexadecapole level for non-hydrogen atoms and up to the quadrupole level for hydrogen atoms), all the minima of $\phi(\boldsymbol{r})$ are significantly reduced and the $\phi(\boldsymbol{r})$ maps loose most of their detail when the multipolar expansion is truncated at the monopole level. Similar effects were found by Stewart and Craven by neglecting higher multipoles when mapping the electrostatic potential of the neurotransmitter γ-aminobutyric acid (GABA).[63b]

Conclusions

We have shown that the topological analysis of the experimental charge density of **1**, described by a pseudoatom multipolar model, have allowed us 1) to obtain a quantitative characterization of the covalent and noncovalent bonding of a relatively large (70 atoms) drug; 2) to reveal both gross and subtle features of $\rho(\boldsymbol{r})$; and 3) to clarify the important features of intra- and intermolecular interactions. In particular, the electrostatic nature of two short S···O and S···N intramolecular contacts that stabilize the overall conformation of LR-B/081 has been established, and their directional "key-lock" character, which faces charge concentrations and charge depletions in the valence shells of sulfur, nitrogen, and oxygen atoms, has been illustrated by means of $\nabla^2\rho(\boldsymbol{r})$ maps. The molecular conformation of **1** in the solid state has been examined in detail and compared with that reported in the literature for other drugs of the same class. Knowledge of the molecular geometry and of the electrostatic potential distribution has allowed us to elucidate the characteristic properties this class of drugs must have to successfully bind to AII receptors.

Many of our findings are based on the experimental values we have obtained for $\rho(\boldsymbol{r})$ and its Laplacian for the crystal. To rely on such values, especially when fine details are involved, very precise measurements of X-ray diffracted intensities are required: thanks to the very low temperature (17 K) and the special care in the treatment of raw data (see the Experimental Section), we believe we have achieved the necessary high level of accuracy and precision. In particular, the inclusion of atomic ADPs for the hydrogen nuclei in the least-squares multipole model seems worth noting. To our knowledge, the charge-density and electrostatic-potential properties presented herein have not been determined experimentally for any other sartan drug or for other drugs of a size similar to that of LR-B/081 by such up-to-date methods.

The extent and accuracy of the results obtained confirm that experimental charge-density studies are well suited to the evaluation of solid-state interactions in large biologically important molecules, which up to now have been very difficult to study by using a fully periodic ab initio approach. The report, in a forthcoming paper, of the experimental evaluation of multipole moments and electrostatic energies for the intermolecular interactions of LR-B/081 can be expected to yield further insights, crucial for studies of molecular modeling and recognition.

Experimental Section

Data collection and reduction: All data were collected from the same crystal, grown from a solution in ethanol. The crystal quality was checked by using diffraction photographs. The sample was mounted on a four-circle Syntex $P\bar{1}$ diffractometer equipped with a Samson cryostat[65] in which the crystal is enclosed in an evacuated, nearly isothermal cavity. The specimen used was the last of a series of six crystals obtained in the same way. The first five of this series were mounted and exposed to X-ray radiation, but none of them reached the final temperature of 17 K without incurring fractures. The last sample was cooled very slowly, at a speed of $1\,\mathrm{deg\,min^{-1}}$ from room temperature to 100 K, and of $0.2\,\mathrm{deg\,min^{-1}}$ from 100 down to 17 K.

Unit-cell dimensions (Table 6) were obtained from the setting angles of 15 medium-angle reflections centered before and after each set of intensity measurements, for a total of 16 times. Intensities were collected at 17(1) K up to a 2θ value of 75° for $Mo_{K\alpha}$ radiation ($\sin\theta/\lambda = 0.86$); the three octants hkl, $hk\bar{l}$, and $h\bar{k}\bar{l}$ were collected in separate steps, with warming in between. The behavior of three standard reflections was peri-

Table 6. Crystallographic data and refinement details for the X-ray analysis of **1**.

empirical formula	$C_{30}H_{30}N_6O_3S$
formula weight	554.66
crystal system	orthorhombic
space group	*Pbca*
a [Å]	29.831(4)
b [Å]	15.505(2)
c [Å]	11.985(1)
V [Å^3]	5543(1)
ρ_{calcd} [g cm^{-3}]	1.329
Z	8
T [K]	17(1)
λ [Å]	0.71073
μ [mm^{-1}]	0.145
crystal size [mm^3]	$0.45\times0.45\times0.125$
$F(000)$	2336
reflections collected/unique reflections	51485/14698
$(\sin\theta/\lambda)_{max}$ [Å^{-1}]	0.86
parameters refined	1633
reflections observed	13812 ($F^2_{obs}>0$)
extinction coefficient [10^{-4} rad^{-1}]	0.52(3)
$R(F)/R(F)^2$ (all data)	0.0299/0.0242
goodness of fit	1.173
$R(F)/R(F)^2$ (for 6144 data with $\sin\theta/\lambda \le 0.65$ Å^{-1})	0.0171/0.0168

odically monitored during each of the three steps of the data collection. Within statistical uncertainty, the three standard reflections behaved in a similar manner and no decay was observed during the 600 h of exposure to X-ray radiation. Low-angle data ($2\theta \leq 25°$) were remeasured at a lower current setting to minimize possible problems associated with non-linearity of the counting system. The total number of intensity measurements was 51485, each recorded with $\omega/2\theta$ scans at a scan rate of 3 deg min^{-1} in 2θ.

Owing to the relatively large dimension of the *a* axis (Table 6), a narrow 2θ-scan range of 1.2° was adopted, but corrections were made for truncation effects which were carefully estimated.[66] Background counts for the weak reflections were averaged over regions of 2θ and the averaged values were applied to all reflections within that region. As these averaged backgrounds had much higher precision than the individual values, the precisions of the net intensities, particularly for the weaker reflections, were appreciably improved.

Corrections were made for Lorentz and polarization effects but not for absorption, which was presumably negligible. Each intensity was assigned a variance $\sigma^2(I)$ based on counting statistics plus an additional term $(0.02S)^2$, where S is the scan count; this term was suggested by the fluctuations in the intensities of the three standard reflections. Weighted averaging of multiple observations yielded 14698 independent values of F^2_{obs}, of which 886 were negative. The value of R(merge) was 0.0246 for the 13812 non-negative reflections measured more than once. The quantity minimized in all least-squares calculations was $\varepsilon = \Sigma w(F^2_o - k^2F^2_c)^2$, based on all positive reflections, with weights (w) obtained by summing $\sigma^{-2}(F^2_o)$ over the contributing measurements. All crystallographic details are given in Table 6.

In order to test the suitability of CCD Area Detectors for accurate electron-density studies, the same crystal sample was used to collect X-ray diffraction data on a SMART CCD area detector at 120 K.[21]

Refinements: After a preliminary least-squares refinement with the conventional, spherical atom model, the multipole formalism of Stewart[22] was introduced to take into account the asphericity in the electron distributions. Several different multipolar models were tested. The most satisfactory model included multipoles up to the hexadecapole level for the sulfur, oxygen, nitrogen, and carbon atoms and up to the quadrupole level for the hydrogen atoms. The generalized scattering factors (GSF) for the monopoles of these species were computed from the Hartree–Fock atomic functions tabulated by Clementi.[67] Electron-population parameters of inner monopoles were constrained to be equal for all 40 non-hydrogen atoms. Radial terms for the higher multipoles were of the form $r^n\exp(-\alpha r)$: for oxygen, nitrogen, and carbon atoms we have adopted values of $n = 2$, 2, 3, and 4 for dipole, quadrupole, octupole, and hexadecapole, respectively, while for the sulfur atom we used a value of $n = 4$ for all high multipoles. Values of κ and α, as obtained from some preliminary least-squares refinements, are reported in the Supporting Information. Initial scattering factors for hydrogen were those of the H_2 molecule,[68] and their coordinates and isotropic U values were allowed to shift; subsequently, the coordinates of hydrogen atoms were kept fixed and generalized monopole and dipole functions were introduced ($n = 0$ for the monopole and 1 for the dipoles). Finally, anisotropic U_{ij} values (ADPs) were introduced for the 30 hydrogen atoms based on spectroscopic information and the molecular rigid-body librations derived from the refined ADPs of the carbon and nitrogen atoms.[57] Quadrupoles, with $n = 2$, could then also be introduced for the hydrogen atoms. α_0 and α_1 values for the hydrogen atoms were initially set to the standard molecular value of 2.48 bohr^{-1} and then refined (see the Supporting Information for their final values). An isotropic extinction parameter of type I and Lorentzian distribution (in the formalism of Becker and Coppens[69]) was also refined.

The total number of parameters was 1633, comprising the extinction parameter, 360 positional and displacement parameters for the 40 non-hydrogen atoms of the molecule, and 1272 electron-population parameters (1002 for the sulfur, oxygen, nitrogen, and carbon atoms and 270 for the 30 hydrogen atoms). The overall scale factor was not among the refinable parameters; it was estimated at the end of each cycle as the sum of all monopole populations divided by $F(000) = 2336e$.

All refinements were carried out with the VALRAY set of programs,[41] based on the 13812 reflections with $F^2_{obs} > 0$. Despite the large size of the molecule, no constraint between the parameters, besides that on the inner monopoles, was deemed necessary as the ratio $N_{observations}/N_{variables} = 8.46$ was considered sufficiently high.

Convergence was assumed when the absolute value of the relative variation of ε in two subsequent cycles was $\leq 10^{-6}$. All second derivatives were included in the last cycles in order to insure convergence to the correct minimum.

The problem of correlation: A crucial and often neglected point in any multipole analysis of X-ray diffraction data is the problem of correlation, mostly between coordinates and dipole parameters, as well as between the U_{ij} values and the quadrupole terms. As already noted,[20] correlation becomes negligible when high-resolution and low-temperature data are used. In the present case, there were only 67 correlation coefficients greater than the usual threshold value of 0.707 (in absolute value) at the end of the least-squares refinement, rather few compared with the large number of variables (1633). Of these 67 coefficients, 59 did not exceed 0.800, while the remaining 8 are in the range 0.800–0.821. The two largest coefficients (0.821 and 0.811) relate a quadrupole component to the corresponding ADP for a nitrogen and an oxygen atom, respectively. Only one of these 67 coefficients involved a carbon atom, and only three involved hydrogen atoms. Generally, the quantities that suffer the existence of some significant correlation coefficients are the estimated standard deviations, which tend to increase, but in the present work, fractional coordinates and ADPs for non-hydrogen atoms have been determined with high precision (su of 5×10^{-5}–5×10^{-4} and 4×10^{-5}–1×10^{-4} Å^2, respectively). It can be stated that, thanks to the low temperature of 17 K, the size of our data set ($(\sin\theta/\lambda)_{max} = 0.86$) is sufficiently large that correlation problems are not too severe.

Thermal motion: The Hirshfeld rigid-bond test[70] and TLS rigid-body analysis[71] were performed in order to investigate the quality of the refined ADPs. The first test showed that in LR-B/081 the differences between the mean-square displacement amplitudes (MSDA) along bond directions have a mean value of 0.00032 Å^2, well below the limit (0.001 Å^2) suggested by Hirshfeld as indicative of an adequate agreement with the rigid-bond postulate. In particular, only two Δ values, in the O2–C11 ($\Delta = 0.0012$ Å^2) and N2–C5 ($\Delta = 0.0011$ Å^2) bonds, marginally exceed that limit.

The results of the TLS analysis confirm that the whole molecule, as expected, cannot be considered as a unique rigid body. Indeed, a single fitting of molecular ***T***, ***L***, and ***S*** to all the atomic ***U*** tensors gave calculated U_{ij} values differing from the observed ones by, on average, about 9 su. On the other hand, when the fit was performed over individual, separated fragments (thiophene group, pyrimidinone plus butylic chain, phenyls, and tetrazole), a much better agreement was reached ($\langle\Delta U\rangle \approx 1.5$ su). Somewhat irrespective of the number of atoms assumed to form a rigid fragment, the corrections to bond lengths due to the librational motion amount to less than 0.002 Å. Throughout the paper we have reported the experimental values of bond distances uncorrected for thermal motion.

ADPs for the 30 hydrogen atoms of **1** have been obtained following the procedure of Roversi and Destro.[57] As an approximate check of the values obtained, equivalent U values were compared with the previously refined X-ray U_{iso} values: the difference exceeded 2.5 su in only one case, the average $|\Delta/\sigma|$ value being 1.1. These hydrogen-calculated ADPs were included, and kept fixed, in the least-squares refinement, thus allowing the addition of quadrupoles to the multipolar expansion of the hydrogen atoms.

CCDC-207037 contains the supplementary crystallographic data for this paper. These data can be obtained free of charge from the Cambridge Crystallographic Data Centre via www.ccdc.cam.ac.uk/data_request/cif.

Acknowledgements

Financial support of this work by the Italian MURST is gratefully acknowledged. We also thank Dr. A. Salimbeni of Istituto Lusofarmaco, Italy, for the provision of crystals, Dr. P. Roversi for valuable suggestions and discussions, and Dr. C. Flensburg for substantial help with a special version of the VALRAY package.

[1] a) R. R. Wexler, W. J. Greenlee, J. D. Irvin, M. R. Goldberg, K. Prendergast, R. D. Smith, P. B. M. W. M. Timmermans, *J. Med. Chem.* **1996**, *39*, 625–656; b) J. L. Reid, P. C. Rubin, *Physiol. Rev.* **1987**, *67*, 725–745.

[2] D. J. Carini, J. V. Duncia, P. E. Aldrich, A. T. Chiu, A. L. Johnson, M. E. Pierce, W. A. Price, J. B. Santella, III, G. J. Wells, R. R. Wexler, P. C. Wong, S. E. Yoo, P. B. M. W. M. Timmermans, *J. Med. Chem.* **1991**, *34*, 2525–2547.

[3] a) L. Polevaya, T. Mavromoustakos, P. Zoumboulakis, S. G. Grdadolnik, P. Roumelioti, N. Giatas, I. Mutule, T. Keivish, D. V. Vlahakos, E. K. Iliodromitis, D. Th. Kremastinos, J. Matsoukas, *Bioorg. Med. Chem.* **2001**, *9*, 1639–1647; b) Y. Nagao, T. Hirata, S. Goto, S. Sano, A. Kakehi, K. Iizuka, M. Shiro, *J. Am. Chem. Soc.* **1998**, *120*, 3104–3110; c) H. Yanagisawa, Y. Amemiya, T. Kanazaki, Y. Shimiji, K. Fujimoto, Y. Kitahara, T. Sada, M. Mizuno, M. Ikeda, S. Miyamoto, Y. Furukawa, H. Koike, *J. Med. Chem.* **1996**, *39*, 323–338; d) K. Kubo, Y. Inada, Y. Kohara, Y. Sugiura, M. Ojima, K. Itoh, Y. Furukawa, K. Nishikawa, K. Naka, *J. Med. Chem.* **1993**, *36*, 1772–1784.

[4] a) B. C. Wilkes, L. Masaro, P. W. Shiller, K. A. Carpenter, *J. Med. Chem.* **2002**, *45*, 4410–4418; b) E. Theodoropoulou, D. Marsh, *Biochim. Biophys. Acta* **1999**, *1461*, 135–146.

[5] a) E. M. Krovat, T. Langer, *J. Med. Chem.* **2003**, *46*, 716–726; b) A. Kurup, R. Garg, D. J. Carini, C. Hansch, *Chem. Rev.* **2001**, *101*, 2727–2750; c) T. Mavromoustakos, A. Kolocouris, M. Zervou, P. Roumelioti, J. Matsoukas, R. Weisemann, *J. Med. Chem.* **1999**, *42*, 1714–1722; d) L. Belvisi, L. Bonati, G. Bravi, D. Pitea, C. Scolastico, A. Vulpetti, *J. Mol. Struct. Theochem* **1993**, *281*, 237–252.

[6] A. Salimbeni, R. Canevotti, F. Paleari, D. Poma, S. Caliari, F. Fici, R. Cirillo, A. R. Renzetti, A. Subissi, L. Belvisi, G. Bravi, C. Scolastico, A. Giachetti, *J. Med. Chem.* **1995**, *38*, 4806–4820.

[7] R. Cirillo, A. R. Renzetti, P. Cucchi, M. Guelfi, A. Salimbeni, A. Subissi, A. Giachetti, S. Caliari, A. Castellucci, S. Evangelista, *Br. J. Pharmacol.* **1995**, *114*, 1117–1124.

[8] R.-M. Catalioto, R. Porchia, A. R. Renzetti, M. Criscuoli, A. Subissi, A. Giachetti, *Eur. J. Pharmacol.* **1995**, *280*, 285–292.

[9] A. R. Renzetti, M. Criscuoli, A. Salimbeni, A. Subissi, *Eur. J. Pharmacol. Mol. Pharmacol. Sect.* **1995**, *290*, 151–156.

[10] A. Salimbeni, F. Paleari, *Top. Heterocycl. Syst.: Synth., React. Prop.* **1996**, *1*, 63–86.

[11] R. Mancina, T. Susini, A. R. Renzetti, G. Forti, E. Razzoli, M. Serio, M. Maggi, *J. Clin. Endocrinol. Metab.* **1996**, *81*, 1753–1757.

[12] D. Notarangelo, P. Ghetti, R. Stradi, A. Salimbeni, E. Pini, *Boll. Chim. Farm.* **1997**, *136*, 474–481.

[13] R. Destro, R. Soave, *Acta Crystallogr. Sect. C* **1995**, *51*, 1383–1385.

[14] R. Soave, R. Destro, L. Belvisi, C. Scolastico in *Electron, Spin and Momentum Densities and Chemical Reactivity* (Eds.: P. G. Mezey, B. E. Robertson), Kluwer Academic Publishers, Dordrecht, The Netherlands, **2000**, pp. 275–283.

[15] The temperature of the data collection performed in 1994 has been earlier reported erroneously as 18(1) K (e.g., in refs. [14] and [21]).

[16] R. F. W. Bader, *Atoms in molecules: a quantum theory*, Oxford University Press, Oxford, **1990**.

[17] a) T. S. Koritsanszky, P. Coppens, *Chem. Rev.* **2001**, *101*, 1583–1627; b) P. Coppens, *X-ray Charge Densities and Chemical Bonding*, Oxford University Press, New York, **1997**.

[18] F. K. Larsen in *The Application of Charge Density Research to Chemistry and Drug Design* (Eds.: G. A. Jeffrey, J. F. Piniella), Plenum, New York, **1991**, pp. 187–208.

[19] P. Coppens, Y. Abramov, M. Carducci, B. Korjov, I. Novozhilova, C. Alhambra, M. R. Pressprich, *J. Am. Chem. Soc.* **1999**, *121*, 2585–2593.

[20] R. Destro, P. Roversi, M. Barzaghi, R. E. Marsh, *J. Phys. Chem. A* **2000**, *104*, 1047–1054.

[21] P. Macchi, D. M. Proserpio, A. Sironi, R. Soave, R. Destro, *J. Appl. Crystallogr.* **1998**, *31*, 583–588.

[22] R. F. Stewart, *Acta Crystallogr. Sect. A* **1976**, *32*, 565–574.

[23] a) R. Destro, R. E. Marsh, R. Bianchi, *J. Phys. Chem.* **1988**, *92*, 966–973; b) R. Destro, F. Merati, *Acta Crystallogr. Sect. B* **1995**, *51*, 559–570; c) P. Roversi, M. Barzaghi, F. Merati, R. Destro, *Can. J. Chem.* **1996**, *74*, 1145–1161; d) A. Forni, R. Destro, *Chem. Eur. J.* **2003**, *9*, 5528–5537.

[24] M. N. Burnett, C. K. Johnson, ORTEPIII, *Oak Ridge Thermal Ellipsoid Plot Program for Crystal Structure Illustrations*, Oak Ridge National Laboratory Report ORNL-6895, Oak Ridge, Tennessee, USA, **1996**.

[25] G. A. Jeffrey, J. R. Ruble, R. K. McMullan, J. A. Pople, *Proc. R. Soc. London, Ser. A* **1987**, *414*, 47–57.

[26] a) J. L. Baudour, L. Toupet, Y. Délugeard, S. Ghémid, *Acta Crystallogr. Sect. C* **1986**, *42*, 1211–1217; b) A. Almenningen, O. Bastiansen, L. Fernholt, *J. Mol. Struct.* **1985**, *128*, 59–76; c) S. Tsuzuki, K. Tanabe, *J. Phys. Chem.* **1991**, *95*, 139–144.

[27] F. H. Allen, O. Kennard, D. G. Watson, L. Brammer, A. G. Orpen, R. Taylor in *International Tables for Crystallography*, *Vol. C* (Ed.: A. J. C. Wilson), Kluwer Academic Publishers, Dordrecht, The Netherlands, **1995**, p. 696.

[28] D. Cremer, J. A. Pople, *J. Am. Chem. Soc.* **1975**, *97*, 1354–1358.

[29] F. H. Allen, *Acta Crystallogr. Sect. B* **2002**, *58*, 380–388.

[30] Z. Böcskei, K. Simon, R. Rao, A. Caron, C. A. Rodger, M. Bauer, *Acta Crystallogr. Sect. C* **1998**, *54*, 808–810.

[31] a) D. Fernández, D. Vega, J. A. Ellena, G. Echeverría, *Acta Crystallogr. Sect. C* **2002**, *58*, m418–m420; b) A. L. Johnson, D. J. Carini, A. T. Chiu, J. V. Duncia, W. A. Price, Jr., G. J. Wells, R. R. Wexler, P. C. Wong, P. B. M. W. M. Timmermans, *Drug News & Perspect.* **1990**, *3*, 337–351.

[32] a) M. Mascal, *Chem. Commun.* **1998**, 303–304; b) A. Bondi, *J. Phys. Chem.* **1964**, *68*, 441–451.

[33] a) B. M. Goldstein, F. Takusagawa, H. M. Berman, P. C. Srivastava, R. K. Robins, *J. Am. Chem. Soc.* **1983**, *105*, 7416–7422; b) P. Franchetti, L. Cappellacci, M. Grifantini, A. Barzi, G. Nocentini, H. Yang, A. O'Connor, H. N. Jayaram, C. Carrell, B. M. Goldstein, *J. Med. Chem.* **1995**, *38*, 3829–3837; c) H. Li, W. A. Hallows, J. S. Punzi, V. E. Marquez, H. L. Carrell, K. W. Pankievicz, K. A. Watanabe, B. M. Goldstein, *Biochemistry* **1994**, *33*, 23–32.

[34] a) G. A. Jeffrey, *An Introduction to Hydrogen Bonding*, Oxford University Press, Oxford, **1997**; b) G. R. Desiraju, T. Steiner, *The Weak Hydrogen Bond*, Oxford University Press, Oxford, **1999**; c) T. Steiner, *Angew. Chem.* **2002**, *114*, 50–80; *Angew. Chem. Int. Ed.* **2002**, *41*, 48–76.

[35] A. L. Llamas Saiz, C. Foces-Foces, *J. Mol. Struct.* **1990**, *238*, 367–382.

[36] W. Shin, T.-S. Yoon, S. E. Yoo, *Acta Crystallogr. Sect. C* **1996**, *52*, 1019–1022.

[37] P. Coppens, P. J. Becker in *International Tables for Crystallography*, *Vol. C* (Ed.: A. J. C. Wilson), Kluwer Academic Publishers, Dordrecht, The Netherlands, **1995**, p. 628.

[38] A. Kirfel, A. Gupta, G. Will, *Acta Crystallogr. Sect. B* **1979**, *35*, 2291–2300.

[39] V. Pichon-Pesme, C. Lecomte, H. Lachekar, *J. Phys. Chem.* **1995**, *99*, 6242–6250.

[40] a) R. F. W. Bader, K. F. Laidig, *Trans. Am. Crystallogr. Assoc.* **1990**, *26*, 1–21; b) R. F. W. Bader, K. F. Laidig in *The Application of Charge Density Research to Chemistry and Drug Design* (Eds.: G. A. Jeffrey, J. F. Piniella), Plenum, New York, **1991**, pp. 23–62.

[41] VALRAY User's Manual (Version 2.1), R. F. Stewart, M. A. Spackman, C. Flensburg, Carnegie Mellon University and University of Copenhagen, **2000**.

[42] PAMoC (Version 2001.0), Online User's Manual, M. Barzaghi, CNR-ISTM, Milano, **2001**.
[43] R. Destro, T. J. Kistenmacher, R. E. Marsh, *Acta Crystallogr. Sect. B* **1974**, *30*, 79–85.
[44] I. Alkorta, L. Barrios, I. Rozas, J. Elquero, *J. Mol. Struct. Theochem* **2000**, *496*, 131–137.
[45] J. P. Ritchie, *Chem. Phys. Lett.* **2004**, *387*, 243–246.
[46] O. Knop, R. J. Boyd, S. C. Choi, *J. Am. Chem. Soc.* **1988**, *110*, 7299–7301.
[47] For this bond the $-\nabla^2\rho_{bcp}$ value is also significantly lower than expected (see Table 3).
[48] K. L. McCormack, P. R. Mallinson, B. C. Webster, D. S. Yufit, *J. Chem. Soc. Faraday Trans.* **1996**, *92*, 1709–1716.
[49] S. Pillet, M. Souhassou, Y. Pontillon, A. Caneschi, D. Gatteschi, C. Lecomte, *New J. Chem.* **2001**, *25*, 131–143.
[50] D. E. Hibbs, C. J. Austin-Woods, J. A. Platts, J. Overgaard, P. Turner, *Chem. Eur. J.* **2003**, *9*, 1075–1084.
[51] C.-R. Lee, T.-H. Tang, L. Chen, Y. Wang, *Chem. Eur. J.* **2003**, *9*, 3112–3121.
[52] A. Wagner, R. Flaig, B. Dittrich, H. Schmidt, T. Koritsánszky, P. Luger, *Chem. Eur. J.* **2004**, *10*, 2977–2982.
[53] J. Overgaard, D. E. Hibbs, *Acta Crystallogr. Sect. A* **2004**, *60*, 480–487.
[54] Note that for three of them, H5A···O3, H9···N4, and S1···N5, the (3,−1) critical point of $\rho(\boldsymbol{r})$ was easily found even when less extended multipole models, for example, only up to octupoles for carbon, nitrogen, and oxygen atoms and hexadecapoles for the sulfur atom, were adopted to interpret the X-ray data. However, to find the bcp of the S1···O1 short contact, hexadecapoles were also necessary for the other non-hydrogen atoms.
[55] W. Scherer, M. Spiegler, B. Pedersen, M. Tafipolsky, W. Hieringer, B. Reinhard, A. J. Downs, G. S. McGrady, *Chem. Commun.* **2000**, 635–636.
[56] J. Overgaard, B. Schiøtt, F. K. Larsen, B. B. Iversen, *Chem. Eur. J.* **2001**, *7*, 3756–3767.
[57] P. Roversi, R. Destro, *Chem. Phys. Lett.* **2004**, *386*, 472–478.
[58] a) T. Steiner, *Chem. Commun.* **1997**, 727–734, and references therein; b) A. Cappelli, G. Giorgi, M. Anzini, S. Vomero, S. Ristori, C. Rossi, A. Donati, *Chem. Eur. J.* **2004**, *10*, 3177–3183; c) P. J. A. Ribeiro-Claro, P. D. Vaz, *Chem. Phys. Lett.* **2004**, *390*, 358–361; d) R. K. Castellano, *Curr. Org. Chem.* **2004**, *8*, 845–865.
[59] a) E. May, R. Destro, C. Gatti, *J. Am. Chem. Soc.* **2001**, *123*, 12248–12254; b) C. Gatti, E. May, R. Destro, F. Cargnoni, *J. Phys. Chem. A* **2002**, *106*, 2707–2720.
[60] U. Koch, P. L. A. Popelier, *J. Phys. Chem.* **1995**, *99*, 9747–9754.
[61] a) S. S. Surange, G. Kumaran, S. Rajappa, D. Pal, P. Chakrabarti, *Helv. Chim. Acta* **1997**, *80*, 2329–2336; b) J. R. Anacona, J. Gómez, D. Loroño, *Acta Crystallogr. Sect. C* **2003**, *59*, o277–o280; c) M. Domagala, S. J. Grabowski, K. Urbaniak, G. Mlostoń, *J. Mol. Struct.* **2004**, *690*, 69–75.
[62] P. Politzer, J. S. Murray, Z. Peralta-Inga, *Int. J. Quantum Chem.* **2001**, *85*, 676–684.
[63] a) R. F. Stewart, *God. Jugosl. Cent. Kristalogr. (Annual of the Yugoslav Centre of Crystallography)* **1982**, *17*, 1–24; b) R. F. Stewart, B. M. Craven, *Biophys. J.* **1993**, *65*, 998–1005; c) R. F. Stewart in *The Application of Charge Density Research to Chemistry and Drug Design* (Eds.: G. A. Jeffrey, J. F. Piniella), Plenum, New York, **1991**, pp. 63–101.
[64] su in the minima range between 10 and 25 kcal mol^{-1}.
[65] S. Samson, E. Goldish, C. J. Dick, *J. Appl. Crystallogr.* **1980**, *13*, 425–432.
[66] R. Destro, R. E. Marsh, *Acta Crystallogr. Sect. A* **1987**, *43*, 711–718.
[67] "Tables of atomic functions", supplement to IBM: E. Clementi, *IBM J. Res. Dev.* **1965**, *9*, Issue 2.
[68] R. F. Stewart, J. J. Bentley, B. Goodman, *J. Chem. Phys.* **1975**, *63*, 3786–3793.
[69] P. J. Becker, P. Coppens, *Acta Crystallogr. Sect. A* **1974**, *30*, 129–147.
[70] F. L. Hirshfeld, *Acta Crystallogr. Sect. A* **1976**, *32*, 239–244.
[71] Performed with a local program based on the treatment of a) V. Schomaker, K. N. Trueblood, *Acta Crystallogr. Sect. B* **1968**, *24*, 63–76 and b) J. D. Dunitz, V. Schomaker, K. N. Trueblood, *J. Phys. Chem.* **1988**, *92*, 856–867. The performance of our code has been repeatedly verified by comparison with that of the THMA code: c) V. Schomaker, K. N. Trueblood, *Acta Crystallogr. Sect. B* **1998**, *54*, 507–514.

Received: September 21, 2004
Revised: February 28, 2005
Published online: May 25, 2005